Dalton Transactions

ROYAL SOCIETY OF CHEMISTRY

PAPER

View Article Online
View Journal | View Issue

Check for updates

Cite this: *Dalton Trans.*, 2023, **52**, 17818

Optoelectronic properties of octahedral molybdenum cluster-based materials at a single crystal level†

Elena Segura-Sanchis, Ana Moreno, Fernando Ramiro-Manzano, Roberto Fenollosa, Marta Feliz * and Pedro Atienzar *

Received 3rd August 2023,
Accepted 3rd November 2023

DOI: 10.1039/d3dt02501b

rsc.li/dalton

Octahedral molybdenum (Mo_6) clusters constitute suitable building blocks for the design of promising single crystal materials in the field of optoelectronics. Here, we prepared single crystals composed of hydroxo Mo_6X_8 (X = Br, Cl) cluster complexes interconnected by H-bonding interactions with water molecules and protons. The optoelectronic responses and the absorption and emission spectra of these cluster-based single crystals were acquired upon light irradiation, and they show dependency on the nature of the halogens, with the brominated cluster being the most conductive. A fast photoelectrical response was recorded and it showed remarkable stability after multiple illumination on/off cycles. The results obtained provide relevant information for the development of photonic and optoelectronic devices, sensors and photocatalysts.

Introduction

Octahedral molybdenum clusters have recently emerged as a green alternative for the development of non-noble metal cluster-based functional nanocomposites, with applications in the field of energy conversion, optoelectronics and lighting.[1–8] These cluster entities have six molybdenum atoms interconnected by direct metal–metal bonds,[9] face-capped by eight halogen ligands and linked to six apical ligands with the formula $[\{Mo_6X^i_8\}L^a_6]^n$ (X^i = halogen; L^a = donor ligand; "i" and "a" refer to the face-capping inner and terminal apical ligand, respectively). Outstanding redox and optical properties, such as absorption of light in the UV-visible range and bright emission in the red/near IR region, are intrinsic to these hexametallic clusters. Such features make these inorganic compounds particularly attractive in the design of functional hybrid nanomaterials with applications in nanoarchitectonics.[10]

Since 1945, the treatment of octahedral molybdenum halide clusters with aqueous alkaline solutions led to $\{Mo_6X^i_8\}^{4+}$ (X^i = halogen, sulphur) cluster core materials decorated by apical hydroxide ligands and with a discrete number of water molecules.[11–17] These compounds were initially formulated by Brosset as $[\{Mo_6X^i_8\}(OH)^a_4(H_2O)^a_2]\cdot 12H_2O$ (X^i = Cl, Br), and subsequently Sheldon ascribed the formulation of the cluster complex to $[\{Mo_6X^i_8\}(OH)^a_6]^{2-}$.[18] Originally, the study of these compounds was centered on structural and composition characterization. In the last few years, the optical, conductive and catalytic properties of a few of the $Mo_6X^i_8$ materials have been investigated at powder crystalline and single crystal levels.[11,15,17,19,20] Among them, hydroxo $Mo_6X^i_8$ cluster complexes appear in the crystal structure interconnected by H-bonding interactions with water molecules (Fig. 1). Recently, the determination of the optical properties of $(H_3O)_2[\{Mo_6Br^i_8\}(OH)^a_6]\cdot 10H_2O$ (**MoBr**) single crystals allowed us to identify for the first time their behavior as Fabry–Pérot microresonators.[21] This property represents a proof of concept of a photonic building block employing a Mo_6 cluster crystal.

Instituto de Tecnología Química, Universitat Politècnica de València – Consejo Superior de Investigaciones Científicas (UPV-CSIC), Avd. de los Naranjos s/n, 46022 Valencia, Spain. E-mail: mfeliz@itq.upv.es, pedatcor@itq.upv.es

† Electronic supplementary information (ESI) available: Fig. S1. Time monitoring of the crystalline surface of MoCl single crystals under ambient conditions; Fig. S2. TG/DTG measurements of MoCl single crystals under air; Fig. S3. (a) Powder X-ray diffraction patterns of freshly prepared (black line) and aged (blue line) MoCl single crystals. (b) Powder X-ray diffractograms (from top to bottom) of aged MoCl and MoBr polycrystalline samples and the simulated pattern obtained from MoBr single crystal X-ray diffraction (ref. 15 of the manuscript); Fig. S4. Raman spectra of freshly prepared (black line) and aged (blue line) MoCl single crystals (λ_{exc} = 785 nm); Fig. S5. Evolution of MoCl crystals before and after contact with CH_3CN and CH_2Cl_2; Fig. S6. Dry MoCl crystals and their evolution after contact with $BMIMBF_4$; Fig. S7. Luminescence decay lifetime of MoBr (top) and MoCl (bottom) single crystals (black lines). The red line corresponds to the fitting of a single-exponential decay model; Fig. S8. PL spectra of selected MoCl (red) and MoBr (black) single crystals selected among the >20 single crystal specimens; Fig. S9: Emission wavelengths depending on MoBr single crystal size; Fig. S10. Current–time (I–t) curves under 405 nm LED light with 0.1 Hz light on/off cycles of a single crystal of $MAPbBr_3$ under λ_{exc} = 405 nm. See DOI: https://doi.org/10.1039/d3dt02501b

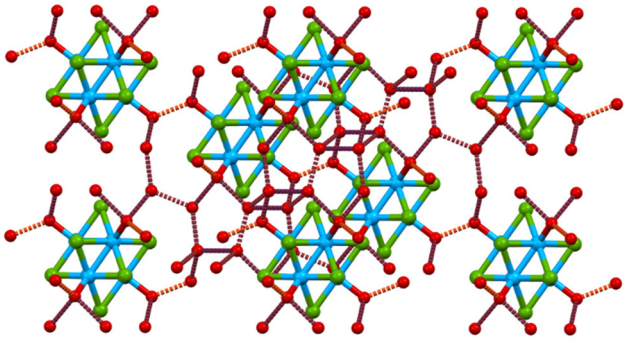

Fig. 1 Schematic representation of H-bonding (dotted lines) in the layers of the **MoBr** structure (atom color code: Mo in blue, Br in green and O in red). H atoms are omitted for clarity.

The electrical characterization of photoactive materials based on Mo_6 clusters with halogens can provide valuable information about their electronic structure and transport properties. In this regard, the electrical properties of **MoBr** and the analogous **MoCl** (X^i = Cl) powdered materials were recently measured and reported.[11] However, such measurements may include contributions from the grain boundaries and the presence of amorphous domains in powdered polycrystalline films.[22] Measurements at the single crystal scale are crucial for gaining insight into these materials. In this work, we synthesized **MoBr** and **MoCl** single crystals and studied their optical and optoelectronic properties. Stability tests and X-ray powder diffraction (XRPD), Raman and thermogravimetric (TG) analyses of **MoCl** single crystals were performed to assess the integrity of the material during optoelectronic measurements.

Results and discussion

We synthesized **MoBr** and **MoCl** single crystals by the treatment of molybdenum halide cluster precursors in aqueous basic media. **MoBr** crystals were obtained in triethylamine/water mixtures, following a methodology reported by us.[21] Single crystals of **MoCl** (≤80 μm) were grown after a slow hydrolysis reaction between $[\{Mo_6Cl^i_8\}Cl^a_6]^{2-}$ and ammonium hydroxide until pH 10.0–11.5, following a similar methodology described by Sheldon.[13] Higher pH values produced a gelatinous suspension and concomitant degradation of the cluster material. Whereas the **MoBr** crystalline material remains stable for at least 2 years under air conditions and light radiation,[21] the $Mo_6Cl^i_8$ cluster material involving water and/or hydroxide groups loses water very easily.[13] It was reported previously that the exposition of **MoCl** to vacuum conditions for several hours promotes the dehydration of the solvation molecules, and the color of the crystals changes from yellow to orange after heating at 67–100 °C.[13] Moreover, heating **MoCl** at 120 °C promotes the dehydration of the material, with a loss of *ca.* 18 water molecules.[11] To prevent deviations of the optical and photoelectrical measurements associated with the decomposition of the crystals, we have monitored the stability of the **MoCl** crystals with time, under ambient conditions and after exposure to selected liquids by using an optical microscope. We observed the appearance of fractures on the crystalline surfaces after 49 h under room conditions (Fig. S1†), which suggests a partial loss of superficial water molecules. X-ray powder diffraction, Raman and TG techniques were used to confirm the robustness of the **MoCl** crystalline material. TG/DTG analysis of **MoCl** evidences a loss of hydration molecules at lower temperature (10 °C, Fig. S2†) compared to that of **MoBr**.[21] Despite the changes observed on the **MoCl** single crystal surfaces, the X-ray patterns confirm the preservation of crystallinity after ageing, and the peaks, associated with the preferential orientation of the single crystals, correspond to the characteristic powder X-ray diffraction pattern (Fig. S3†). The diffraction peaks of the powdered materials confirm that this molybdenum chloride material is isostructural to its brominated analogue (Fig. S3b†), and both structures contain $[\{Mo_6X^i_8\}(OH)^a_6]^{2-}$ clusters interconnected by H-bonding interactions to protons and water molecules.[11,13,18] The Raman spectra of **MoCl** show that the cluster bands remain intact with time under atmospheric conditions (Fig. S4†). The stability of the crystalline surface after contact with liquids with different polarities was monitored by optical inspection. The crystals remained stable after addition to acetonitrile, whereas the presence of dichloromethane cracked drastically the crystalline surface in a short time (1 h), probably due to a fast dehydration or decomposition of the crystals by contact with this solvent (Fig. S5†). After exposition to 1-butyl-3-methylimidazolium tetrafluoroborate ($BMIMBF_4$), the surface of the crystals appeared slightly cracked, as observed for dry samples, preserving their crystallinity with time (Fig. S6†).

The optical properties of both **MoBr** and **MoCl** materials were investigated. The UV-Vis spectra of the molybdenum cluster-based crystals were recorded by diffuse reflectance, and showed a broad absorption band with maxima at *ca.* 300 nm and a long absorption tail until 580 nm (Fig. 2a). **MoCl** shows a wide absorption from the UV to the visible region, and the spectrum of **MoBr** depicts, in addition, a shoulder at 490 nm. Considering time-dependent density functional theory (TD-DFT) calculations carried out on $[\{Mo_6X^i_8\}L^a_6]^{2-}$ (X^i = Cl, Br, I; L^a = F, Cl, Br, I, OH, H_2O) compounds, the most intense band absorption located at *ca.* 300 nm can be ascribed to metal–metal and metal–halogen excitation, whereas the region from *ca.* 350 to 550 nm can also include electronic transitions involving orbitals localized at the $\{Mo_6X^i_8\}^{4+}$ core and apical ligands.[20,24,25] The PL of $Mo_6X^i_8$ crystals was characterized of using steady-state and time-resolved techniques (see the ESI†). Steady-state PL spectra of polycrystalline samples showed emission maxima at 740 nm for X^i = Br, and at 752 nm for X^i = Cl, (Fig. 2b), attributed to the characteristic phosphorescence emission from the triplet state of $\{Mo_6X^i_8\}^{4+}$ cluster cores, produced by intersystem crossing upon photoexcitation of the lowest energy excited singlet state.[19] Time resolved luminescence decay curves of **MoCl** and **MoBr** show lifetimes of 13.7 and 80.9 μs, respectively (Fig. 2b and S7†). These lifetimes are

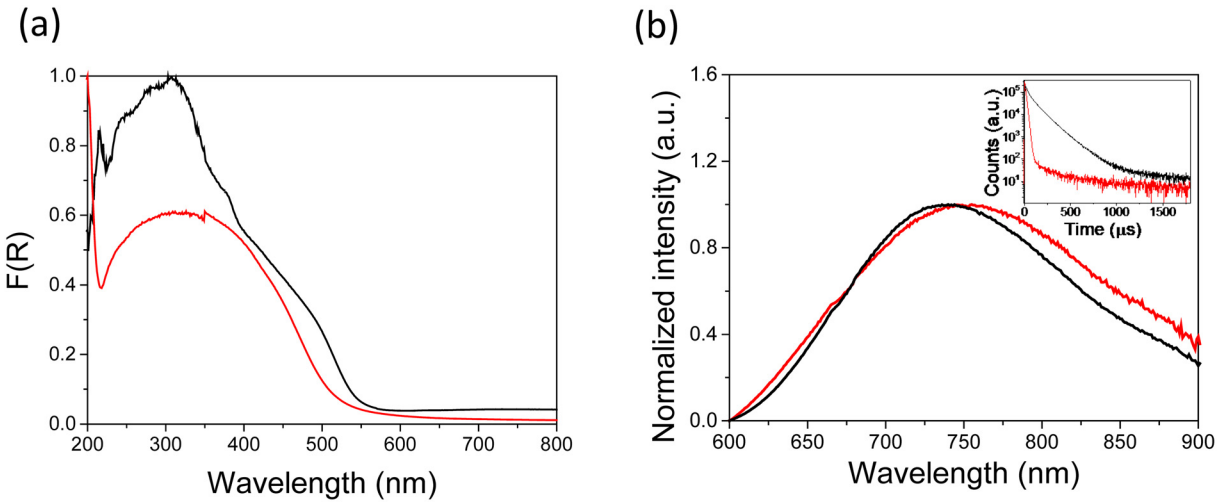

Fig. 2 (a) Diffuse reflectance and (b) steady state PL of a collection of **MoBr** (black line) and **MoCl** (red line) single crystals, registered at λ_{exc} = 405 nm under room conditions. The inset shows the time-resolved PL monitored at 720 nm.

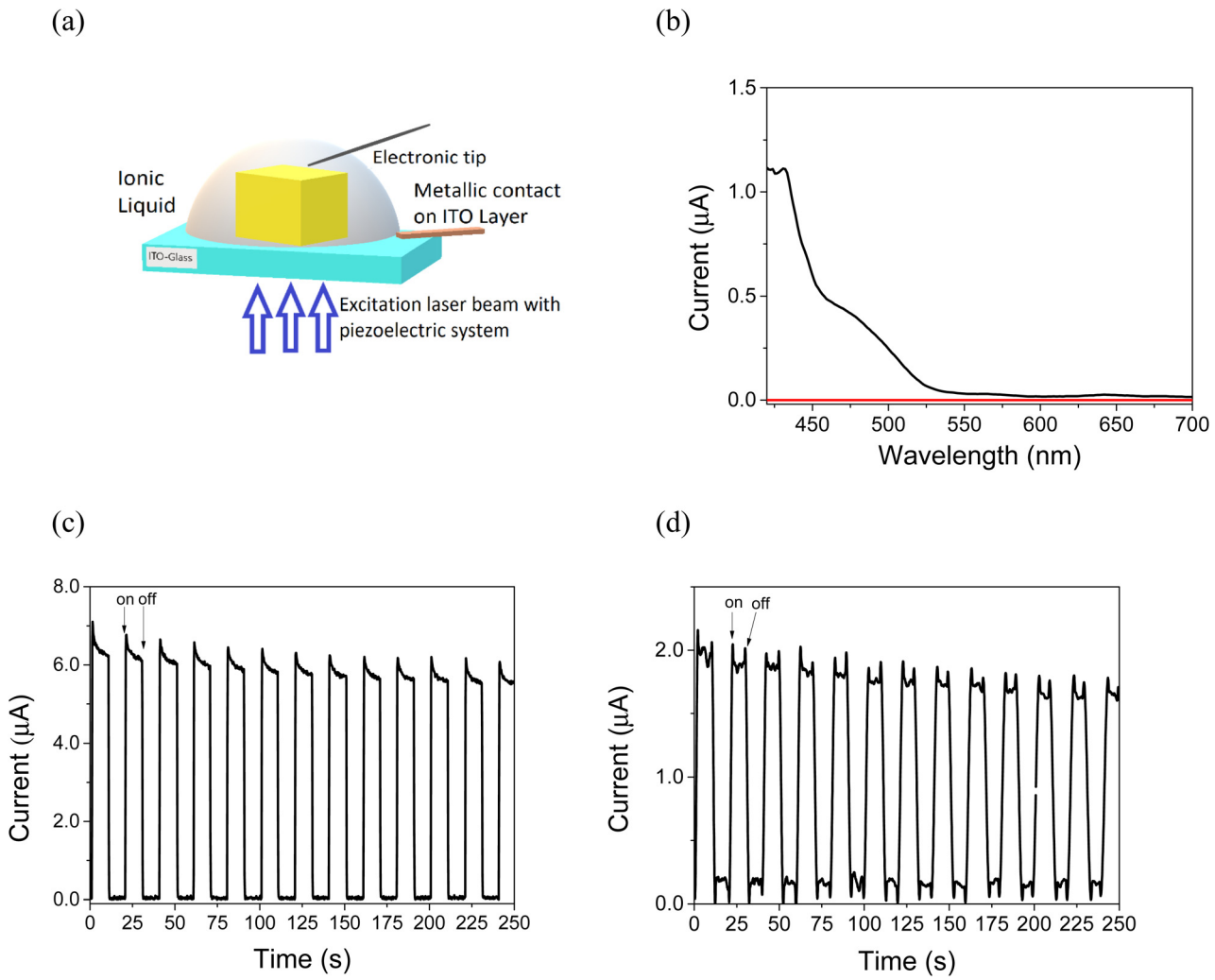

Fig. 3 (a) Experimental scheme of the single crystal contact; (b) photocurrent spectra of a single crystal of **MoBr** embedded into $BMIMBF_4$ (black line) and a drop of $BMIMBF_4$ as a blank (red line), under excitation with a supercontinuum laser at different wavelengths; (c) **MoBr** and (d) **MoCl** current–time (I–t) curves under 405 nm LED light with 0.1 Hz light on/off cycles.

approximately on the same order of magnitude as those reported for $[\{Mo_6X^i_8\}X^a_6]^{2-}$ (X^i = X^a = Cl, Br) crystalline compounds.[20,23] Interestingly, the emission maxima of polycrystalline **MoBr** (740 nm) differ from those reported previously for other samples with similar composition (670 nm),[15,21] probably related to morphological reasons that would be studied in a follow-up work. The emission spectra of single crystals (Fig. S8 and S9†) are within the range of their polycrystalline counterparts (Fig. 2B) for both **MoCl** and **MoBr** samples, and we did not find any correlation between the type of the halogen in the samples and the emission. However, we found a dependence of the wavelength at which the maximum emission occurs on the crystal size (Fig. S9†). Indeed, the phosphorescence shifts to red as the crystal size increases.

Photoconductive measurements of Mo_6-based single crystals were performed under atmospheric conditions. It should be noted that, due to the low electrical conductivity of the powdered polycrystalline materials,[11] it was necessary to embed the single crystals in $BMIMBF_4$, as a non-volatile and conductive electrolyte. The disposition of the crystals during the photoelectric measurements is depicted in Fig. 3a. Fig. 3b shows the photocurrent spectrum of a selected **MoBr** single crystal by scanning the electrical current generated by excitation light from 400 to 800 nm wavelength. Here, the single crystal was deposited in an Indium Tin Oxide (ITO) substrate. The electrical circuit is established by employing a probe tip that comes in contact with the top surface of the crystal. This method enables the selection of the crystal structure and fine positioning of the top contact while eliminating the need for lithographically structured back-contact electrodes and precise transfer positioning. The obtained photocurrent displays a broad band between 400 and 550 nm and a less intense long tail up to 600 nm, corresponding to the characteristic absorption band of this $Mo_6Br^i_8$-based material. These results confirm the photoelectric activity of **MoBr** single crystals under visible light. Among both halide materials, the **MoBr**

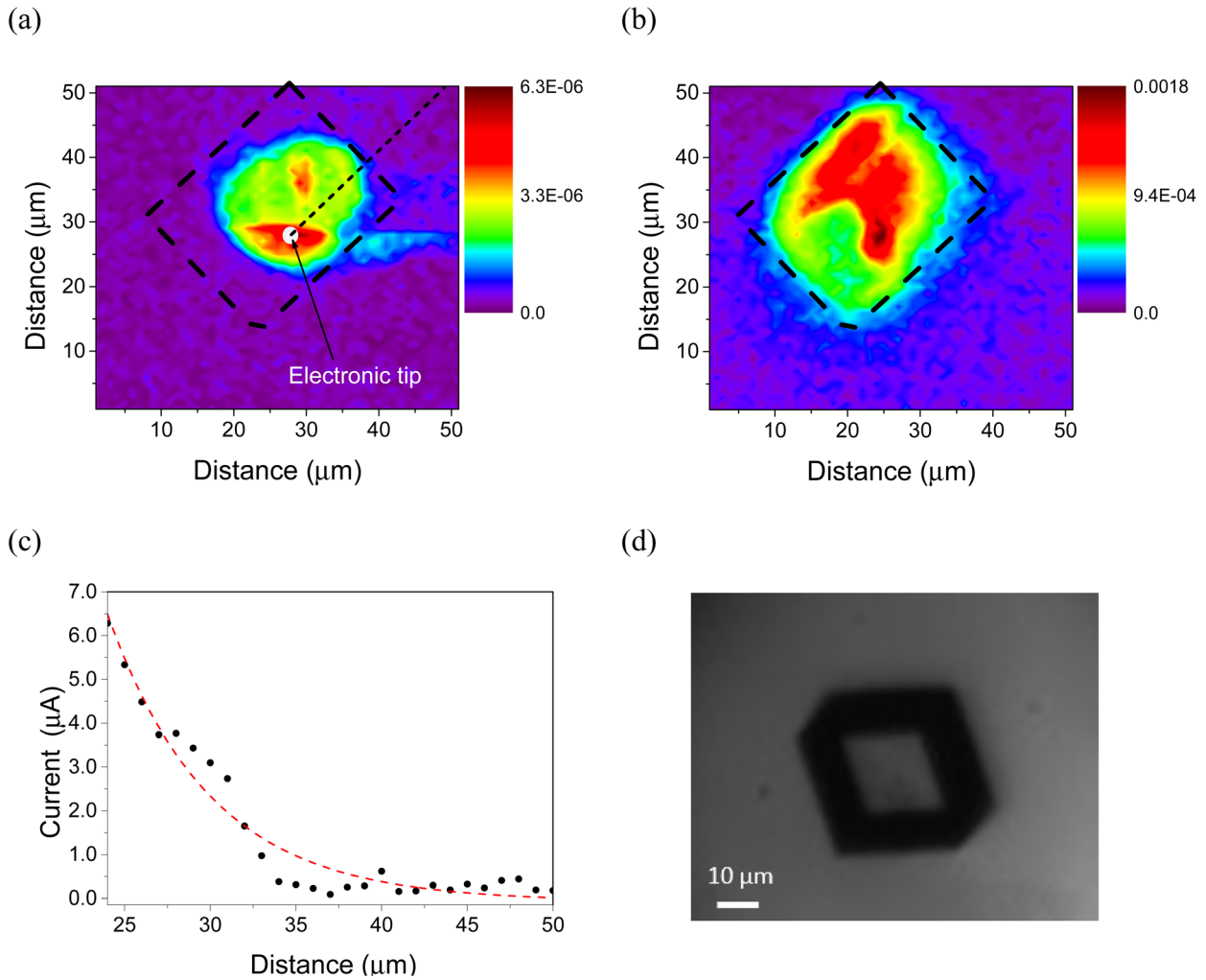

Fig. 4 (a) Photocurrent mapping of a **MoBr** single crystal embedded in $BMIMBF_4$; (b) PL map of the **MoBr** single crystal. Both measurements were performed at room temperature with excitation using a 405 nm diode laser; (c) photocurrent profile along the dashed line depicted in (a). The maximum value corresponds to the electronic tip contact; (d) optical microscopy image of a single crystal of **MoBr** cluster.

single crystals provided the best photoresponse, which may be related to the superior conductivity of the bromide with respect to the chloride cluster material. In contrast, the resistance reported for powdered materials shows that the bromide material is slightly more resistive than the chloride material under ambient conditions, whereas both are on the same order of magnitude.[11] The photostability of the crystals was assessed by photocurrent experiments. The photocurrent measurements, performed with on/off 405 nm light-emitting diode (LED) light exciting cycles (more than 10 times), Fig. 3c, indicate that the current remains constant for both **MoBr** and **MoCl** single crystals after 250 seconds of irradiation (Fig. 3c and d, respectively). This stability of the photoelectric response can be compared to that registered from the single crystal of the $MAPbBr_3$ (MA = methyl ammonium, Fig. S10†) perovskite.[26] The conductivity values achieved under photoirradiation of selected single crystals (*ca.* 2.28 and 8 kΩ for the bromide and chloride cluster materials, respectively) confirm that the **MoBr** crystal shows better conductivity than the chloride analogue.

The photocurrent map (Fig. 4a) registered for a **MoBr** single crystal (Fig. 4d) shows the corresponding spatial variation of the generated current when light from a 405 nm wavelength laser is focused on different positions across the crystal bottom surface (Fig. 4a). The higher intensity values (red color) correspond to the scenario where the position of the light spot matches electrical contact. The greater the horizontal distance between the light source and the electrical tip, the longer the electron transport path, resulting in an increase in the recombination. As a result, at a certain distance, the collected photocurrent is negligible. This represents an experiment similar to Scanning Photocurrent Microscopy (SPCM) where the decay of the photocurrent is directly related to the diffusion length.[27] Since both the 3D rhombohedral crystal geometry and the non-planar configuration of the electrodes do not seem to match the simplicity of the 2D configuration observed from SPCM,[28,29] a quantitative value of diffusion length cannot be reliably extracted. Nevertheless, and under our sample and characterization conditions, a qualitative photocurrent decay was achieved on the order of the micrometers (Fig. 4a and c). This value is in the range of the diffusion lengths of other well-known semiconductors such as hybrid perovskites,[30] $Cu(In, Ga)Se_2$[31] or GaAs.[32] It should be noted that optical phenomena, such as the behavior of an optical cavity, can have a significant influence on the diffusion length.[33,34] In addition, intrinsic defects or impurities and extrinsic properties (doping concentration) may also have an impact on this value.[34] We also measured the PL map (Fig. 4b), which shows the spatial distribution of the PL over the microcrystal, with a maximum emission in the middle-area and some scattered light at the edges. This experiment permits us to characterize the homogeneity/inhomogeneity of the material in terms of emission, which could have an impact on the differences in the photocurrent decay rates along the sample. The distribution of the photocurrent is prominent in the area with electrical contact with the substrate (Fig. 2(a) and (d)), and this area corresponds to the maximum PL emission.

Conclusions

Optical and optoelectronic characterization of aquahydroxo $Mo_6X^i_8$ (X^i = Cl and Br) cluster-based single crystals is reported. These materials are composed of $[\{Mo_6X^i_8\}(OH)^a_6]^{2-}$ complexes interconnected by water molecules and protons through H-networks. These crystals were prepared and crystallized in alkaline aqueous solutions and they remained stable under air and after contact with selected polar liquids. Their PL is dependent on the inner halogen for a collection of single crystals: the emission shifts to longer wavelengths as the electronegativity of the inner halogen increases. Interestingly, the PL of each single crystal shows a dependency on the size and orientation of the crystals (with respect to the light direction). The lifetime of the molybdenum bromide cluster material is longer than that of the chloride analogue, and both are on the order of microseconds. The photoresponse spectrum of **MoBr** single crystals indicates that these crystals are capable of responding in the visible spectrum. In addition, the halide plays a role in the conductivity of the single crystals, with the bromide cluster material being more conductive than the chloride cluster single crystal material. On/off light excitation cycles for both cluster materials confirmed their stability and fast response, showing the possibility of their use in optoelectronic devices, as sensors and photocatalysts.

Experimental procedure

Chemicals

All the manipulations were performed under room temperature and atmospheric conditions. The **MoBr**, $Cs_2[\{Mo_6Cl^i_8\}Cl^a_6]$ and $MAPbBr_3$ materials were synthesized following reported procedures.[21,26,35] NH_4OH was purchased from commercial resources (25% Supelco), as well as $BMIMBF_4$ (pure, Merck), dichloromethane and acetonitrile (≥99.8% and 99.9%, respectively, Sigma Aldrich). Ultrapure deionized water was obtained from a Milli-Q® EQ 7000 Type 1 purification system.

Instrumentation

The pH measurements were performed with a Mettler Toledo SevenEasy pH meter. Photographs of the crystals were recorded with a Nikon Eclipse LV100 microscope. The absorbance bands of the material were elucidated with an Agilent Cary 60 UV-Vis spectrometer. Lifetime photoluminescence measurements on the single crystals were carried out using an inverted microscope, Nikon Ti2-U, equipped with an XY motorized stage. The emission signal was transmitted through optical fibers to an Edinburgh Instruments FLS1100 spectrofluorometer, which was coupled to a cooled photomultiplier (PMT-980). The measurements were performed at room temperature, utilizing a 405 nm excitation wavelength provided by a picosecond (ps) laser diode incorporated into the microscope. The lifetimes (τ) were calculated from the best fitting of the signal to a single-exponential decay ($I(t) = I(0)\exp(-t/\tau)$). A Renishaw inVia Raman Microscope was used to obtain infor-

mation about the microcrystal structure. Crystallographic information of octahedral molybdenum single crystals was obtained using powder X-ray diffraction (CubiX PRO diffractometer, Cu Kα radiation (λ_1 = 1.54060 nm) at 298 K). TG analysis was performed under air conditions. Electrical measurements of Mo_6 crystals were carried out using a home-made system.[36] The crystals were deposited onto a glass substrate and, only in the case of electrical measurements, they were embedded into a drop of $BMIMBF_4$ as a conductive matrix. The spectra were recorded by tip contact to the surface of the crystal and under an excitation laser beam in the perpendicular direction to the plane of deposition of the crystal (Fig. 3a). The crystal was placed between two magnification Mitutoyo objective lenses, the laser beam (405 nm and *ca.* 350 microwatts) was focused on the crystal and the produced current was collected by the system and recorded by a Stanford lock-in amplifier and a FEMTO DLPCA-200 transient impedance device. To provide a broad wavelength coverage, a supercontinuum source coupled to a monochromator was used for the acquisition of the photocurrent spectrum. Two recurrent passes (employing a retroreflector) to a diffraction grating allowed the selected wavelength and removed the chromatic spatial dispersion (for appropriate focusing). The focusing objective is positioned employing a three axis piezo system. This was employed to move the excitation laser through the crystal surface. The current–time (I–t) curves were registered under 405 nm light-emitting diode (LED) light with 0.1 Hz light on/off. The conductivity values were acquired under photoirradiation and applying a −1.26 V bias.

Synthetic procedure

The preparation of crystals was performed by the hydrolysis of $Cs_2[Mo_6Cl^i_8Cl^a_6]$. This precursor (20 mg) was dispersed in water (6 mL) in a glass beaker (25 mL) at room temperature and with continuous stirring. The pH of the suspension was monitored with a slow addition of NH_4OH, with pH values ranging from 2.0–3.5 to 10.0–11.5. A transparent yellow solution was obtained, and then, the flask was covered with an inverted beaker and left to undergo slow crystallization at room temperature. After *ca.* 2–5 days, the solution became clear and the resulting crystalline precipitate was thoroughly washed three times with water, by successive decanting. The liquid extractions were filtered with nylon microfilters (0.45 μm pore size), and their identification by UV-vis confirmed the absence of absorption bands characteristic of $Mo_6Cl^i_8$ cluster units in the filtrate. Yellow-orange crystals were isolated with crystal sizes around 20–40 μm. The crystals were kept in water and in a vial protected from light and at low temperature (*ca.* 5 °C). The crystals were analyzed by Raman, XRPD, TG/DTG and luminescence techniques.

Crystal stability study

The stability of selected crystals under environmental conditions was monitored by inspection of their crystalline surface with an optical microscope during specific times. The robustness of selected crystals was also studied towards $BMIMBF_4$, acetonitrile and dichloromethane, by immersion of the crystal into a drop of the chosen solvent.

Author contributions

The manuscript was written through the contributions of all authors. Apart from this, E. S.-S. performed the spectroscopic characterization and photocurrent measurements, A. M. and M. F. prepared and characterized the cluster-based single crystals, F. R-M. and R. F. created and optimized the setup for photocurrent spectra and mapping experiments for micrometrical single crystal structures and contributed in mapping experiments, and M. F. and P. A. contributed to conceptualization, discussions and supervision of the research. All authors have given approval to the final version of the manuscript.

Conflicts of interest

There are no conflict of interest to declare.

Acknowledgements

We would like to thank the technical team at the Instituto de Tecnología Química for providing us all the facilities for all the characterization processes. This research was supported by the project PID2021-123163OB-I00 funded by MCIN/AEI/10.13039/501100011033/and FEDER A way of making Europe and Severo Ochoa Centre of Excellence Program (CEX2021-001230-S). F. R. M. acknowledges CSIC under the program: Ayudas para la incorporación de nuevos Científicos Titulares (Grant No. 202280I200).

References

1 A. Renaud, P.-Y. Jouan, N. Dumait, S. Ababou-Girard, N. Barreau, T. Uchikoshi, F. Grasset, S. Jobic and S. Cordier, Evidence of the Ambipolar Behavior of Mo_6 Cluster Iodides in All-Inorganic Solar Cells: A New Example of Nanoarchitectonic Concept, *ACS Appl. Mater. Interfaces*, 2022, **14**, 1347–1354, DOI: **10.1021/acsami.1c17845**.

2 K. Harada, T. K. N. Nguyen, F. Grasset, C. Comby-Zerbino, L. MacAleese, F. Chirot, P. Dugourd, N. Dumait, S. Cordier, N. Ohashi, M. Matsuda and T. Uchikoshi, Light-dependent ionic-electronic conduction in an amorphous octahedral molybdenum cluster thin film, *NPG Asia Mater.*, 2022, **14**, 21, DOI: **10.1038/s41427-022-00366-8**.

3 T. K. N. Nguyen, F. Grasset, N. Dumait, S. Cordier, D. Berthebaud, N. Ohashi and T. Uchikoshi, Tunable photo-induced electronic property of octahedral metal clusters, *Mater. Lett.: X*, 2021, **11**, 100079, DOI: **10.1016/j.mlblux.2021.100079**.

4 Y. Liang, M. N. Sokolov, M. A. Mikhaylov, H. Ibrahim, M. Goldmann, S. Choua, N. Le Breton, C. Boudon,

V. Badets, A. Bonnefont and L. Ruhlmann, A 3D electropolymerized thin film based on an isoporphyrin and on a pyridine end-decorated molybdenum(II) halide cluster: Photoelectrochemical and impedance properties, *Electrochim. Acta*, 2021, **388**, 138493, DOI: **10.1016/j.electacta.2021.138493**.

5 T. K. N. Nguyen, F. Grasset, S. Cordier, M. Amela-Cortes, Y. Matsui, N. Ohashi, N. Shirahata and T. Uchikoshi, Preparation and characterization of hollow silica nanocomposite functionalized with UV absorbable molybdenum cluster, *Adv. Powder Technol.*, 2020, **31**, 895–903, DOI: **10.1016/j.apt.2019.12.009**.

6 S. Khlifi, J. Bigeon, M. Amela-Cortes, N. Dumait, G. Loas, S. Cordier and Y. Molard, Switchable Two-Dimensional Waveguiding Abilities of Luminescent Hybrid Nanocomposites for Active Solar Concentrators, *ACS Appl. Mater. Interfaces*, 2020, **12**, 14400–14407, DOI: **10.1021/acsami.9b23055**.

7 A. Renaud, F. Grasset, B. Dierre, T. Uchikoshi, N. Ohashi, T. Takei, A. Planchat, L. Cario, S. Jobic, F. Odobel and S. Cordier, Inorganic Molybdenum Clusters as Light-Harvester in All Inorganic Solar Cells: A Proof of Concept, *ChemistrySelect*, 2016, **1**, 2284–2289, DOI: **10.1002/slct.201600508**.

8 A. Renaud, T. K. N. Nguyen, F. Grasset, M. Raissi, V. Guillon, F. Delabrouille, N. Dumait, P.-Y. Jouan, L. Cario, S. Jobic, Y. Pellegrin, F. Odobel, S. Cordier and T. Uchikoshi, Preparation by electrophoretic deposition of molybdenum iodide cluster-based functional nanostructured photoelectrodes for solar cells, *Electrochim. Acta*, 2019, **317**, 737–745, DOI: **10.1016/j.electacta.2019.05.154**.

9 F. A. Cotton, Metal Atom Clusters in Oxide Systems, *Inorg. Chem.*, 1964, **3**, 1217–1220, DOI: **10.1021/ic50019a003**.

10 N. T. K. Nguyen, C. Lebastard, M. Wilmet, N. Dumait, A. Renaud, S. Cordier, N. Ohashi, T. Uchikoshi and F. Grasset, A review on functional nanoarchitectonics nanocomposites based on octahedral metal atom clusters (Nb_6, Mo_6, Ta_6, W_6, Re_6): inorganic 0D and 2D powders and films, *Sci. Technol. Adv. Mater.*, 2022, **23**, 547–578, DOI: **10.1080/14686996.2022.2119101**.

11 G. Daigre, J. Cuny, P. Lemoine, M. Amela-Cortes, S. Paofai, N. Audebrand, A. Le Gal La Salle, E. Quarez, O. Joubert, N. G. Naumov and S. Cordier, Metal Atom Clusters as Building Blocks for Multifunctional Proton-Conducting Materials: Theoretical and Experimental Characterization, *Inorg. Chem.*, 2018, **57**, 9814–9825, DOI: **10.1021/acs.inorgchem.8b00340**.

12 J. C. Sheldon, 76. Bromo- and iodo-molybdenum(II) compounds, *J. Chem. Soc.*, 1962, 410–415, DOI: **10.1039/JR9620000410**.

13 J. C. Sheldon, 208. Chloromolybdenum(II) compounds, *J. Chem. Soc.*, 1960, 1007–1014, DOI: **10.1039/JR9600001007**.

14 M. A. Mikhaylov, P. A. Abramov, V. Y. Komarov and M. N. Sokolov, Cluster aqua/hydroxocomplexes supporting extended hydrogen bonding networks. Preparation and structure of a unique series of cluster hydrates $[Mo_6I_8(OH)_4(H_2O)_2]\cdot nH_2O$ (n=2, 12, 14), *Polyhedron*, 2017, **122**, 241–246, DOI: **10.1016/j.poly.2016.11.011**.

15 M. Feliz, M. Puche, P. Atienzar, P. Concepción, S. Cordier and Y. Molard, In situ generation of active molybdenum octahedral clusters for photocatalytic hydrogen production from water, *ChemSusChem*, 2016, **9**, 1963–1971, DOI: **10.1002/cssc.201600381**.

16 M. Puche, R. García-Aboal, M. A. Mikhaylov, M. N. Sokolov, P. Atienzar and M. Feliz, Enhanced Photocatalytic Activity and Stability in Hydrogen Evolution of Mo6 Iodide Clusters Supported on Graphene Oxide, *Nanomaterials*, 2020, **10**, 1259, DOI: **10.3390/nano10071259**.

17 M. V. Marchuk, N. A. Vorotnikova, Y. A. Vorotnikov, N. V. Kuratieva, D. V. Stass and M. A. Shestopalov, Optical property trends in a family of {Mo6I8} aquahydroxo complexes, *Dalton Trans.*, 2021, **50**, 8794–8802, DOI: **10.1039/D1DT01293B**.

18 J. C. Sheldon, Polynuclear Complexes of Molybdenum(II), *Nature*, 1959, **184**, 1210–1213, DOI: **10.1038/1841210a0**.

19 S. Akagi, T. Horiguchi, S. Fujii and N. Kitamura, Terminal Ligand (L) Effects on Zero-Magnetic-Field Splitting in the Excited Triplet States of $[\{Mo_6Br_8\}L_6]^{2-}$ (L = Aromatic Carboxylates), *Inorg. Chem.*, 2019, **58**, 703–714, DOI: **10.1021/acs.inorgchem.8b02881**.

20 K. Costuas, A. Garreau, A. Bulou, B. Fontaine, J. Cuny, R. Gautier, M. Mortier, Y. Molard, J. L. Duvail, E. Faulques and S. Cordier, Combined theoretical and time-resolved photoluminescence investigations of $[Mo_6Br^i_8Br^a_6]^{2-}$ metal cluster units: evidence of dual emission, *Phys. Chem. Chem. Phys.*, 2015, **17**, 28574–28585, DOI: **10.1039/C5CP03960F**.

21 E. Segura-Sanchís, R. Fenollosa, I. Rodríguez, Y. Molard, S. Cordier, M. Feliz and P. Atienzar, Octahedral Molybdenum Cluster-Based Single Crystals as Fabry–Pérot Microresonators, *Cryst. Growth Des.*, 2022, **22**, 60–65, DOI: **10.1021/acs.cgd.1c01144**.

22 M. A. Haque, J. Troughton and D. Baran, Processing-Performance Evolution of Perovskite Solar Cells: From Large Grain Polycrystalline Films to Single Crystals, *Adv. Energy Mater.*, 2020, **10**, 1902762, DOI: **10.1002/aenm.201902762**.

23 N. Kitamura, Y. Kuwahara, Y. Ueda, Y. Ito, S. Ishizaka, Y. Sasaki, K. Tsuge and S. Akagi, Excited Triplet States of $[\{Mo_6Cl_8\}Cl_6]^{2-}$, $[\{Re_6S_8\}Cl_6]^{4-}$, and $[\{W_6Cl_8\}Cl_6]^{2-}$ Clusters, *Bull. Chem. Soc. Jpn.*, 2017, **90**, 1164–1173, DOI: **10.1246/bcsj.20170168**.

24 R. Ramirez-Tagle and R. Arratia-Pérez, Electronic structure and molecular properties of the $[Mo_6X_8L_6]^{2-}$; X = Cl, Br, I; L = F, Cl, Br, I clusters, *Chem. Phys. Lett.*, 2008, **460**, 438–441, DOI: **10.1016/j.cplett.2008.06.035**.

25 X. Zarate, E. Schott, L. Alvarado-Soto and R. Ramirez-Tagle, A family of octahedral molybdenum cluster complexes $[Mo_6Cl_8(H_2O)_n(OH)_{6-n}]^{n-2}$ with n = 0–6 as a pH-sensors: A theoretical study, *Chem. Phys. Lett.*, 2013, **567**, 39–42, DOI: **10.1016/j.cplett.2013.02.071**.

26 R. García-Aboal, R. Fenollosa, F. Ramiro-Manzano, I. Rodríguez, F. Meseguer and P. Atienzar, Single Crystal Growth of Hybrid Lead Bromide Perovskites Using a Spin-Coating Method, *ACS Omega*, 2018, **3**, 5229–5236, DOI: **10.1021/acsomega.8b00447**.

27 R. Graham and D. Yu, Scanning photocurrent microscopy in semiconductor nanostructures, *Mod. Phys. Lett. B*, 2013, **27**, 1330018, DOI: **10.1142/S0217984913300184**.

28 Y.-C. Wei, C.-H. Chu and M.-H. Mao, Minority carrier decay length extraction from scanning photocurrent profiles in two-dimensional carrier transport structures, *Sci. Rep.*, 2021, **11**, 21863, DOI: **10.1038/s41598-021-01446-5**.

29 B. Yang, J. Chen, Q. Shi, Z. Wang, M. Gerhard, A. Dobrovolsky, I. G. Scheblykin, K. J. Karki, K. Han and T. Pullerits, High Resolution Mapping of Two-Photon Excited Photocurrent in Perovskite Microplate Photodetector, *J. Phys. Chem. Lett.*, 2018, **9**, 5017–5022, DOI: **10.1021/acs.jpclett.8b02250**.

30 L. R. V. Buizza, T. W. Crothers, Z. Wang, J. B. Patel, R. L. Milot, H. J. Snaith, M. B. Johnston and L. M. Herz, Charge-Carrier Dynamics, Mobilities, and Diffusion Lengths of 2D–3D Hybrid Butylammonium–Cesium–Formamidinium Lead Halide Perovskites, *Adv. Funct. Mater.*, 2019, **29**, 1902656, DOI: **10.1002/adfm.201902656**.

31 G. Brown, V. Faifer, A. Pudov, S. Anikeev, E. Bykov, M. Contreras and J. Wu, Determination of the minority carrier diffusion length in compositionally graded Cu(In, Ga)Se_2 solar cells using electron beam induced current, *Appl. Phys. Lett.*, 2010, **96**, 22104, DOI: **10.1063/1.3291046**.

32 K.-S.-A. Butcher, D. Alexiev and T.-L. Tansley, Minority carrier diffusion lengths for high purity liquid phase epitaxial GaAs, *Aust. J. Phys.*, 1993, **46**, 317, DOI: **10.1071/PH930317**.

33 Y. Zhang, C.-K. Lim, Z. Dai, G. Yu, J. W. Haus, H. Zhang and P. N. Prasad, Photonics and optoelectronics using nano-structured hybrid perovskite media and their optical cavities, *Phys. Rep.*, 2019, **795**, 1–51, DOI: **10.1016/j.physrep.2019.01.005**.

34 D. Neamen, *Semiconductor Physics and Devices: Basic Principles/D.A. Neamen*, 2012.

35 N. Saito, P. Lemoine, N. Dumait, M. Amela-Cortes, S. Paofai, T. Roisnel, V. Nassif, F. Grasset, Y. Wada, N. Ohashi and S. Cordier, From $Cs_2Mo_6Cl_{14}$ to $Cs_2Mo_6Cl_{14}{\cdot}H_2O$ and Vice Versa: Crystal Chemistry Investigations, *J. Cluster Sci.*, 2017, **28**, 773–798, DOI: **10.1007/s10876-016-1133-5**.

36 F. Ramiro-Manzano, R. García-Aboal, R. Fenollosa, S. Biasi, I. Rodriguez, P. Atienzar and F. Meseguer, Optical properties of organic/inorganic perovskite microcrystals through the characterization of Fabry–Pérot resonances, *Dalton Trans.*, 2020, **49**, 12798–12804, DOI: **10.1039/D0DT02254C**.